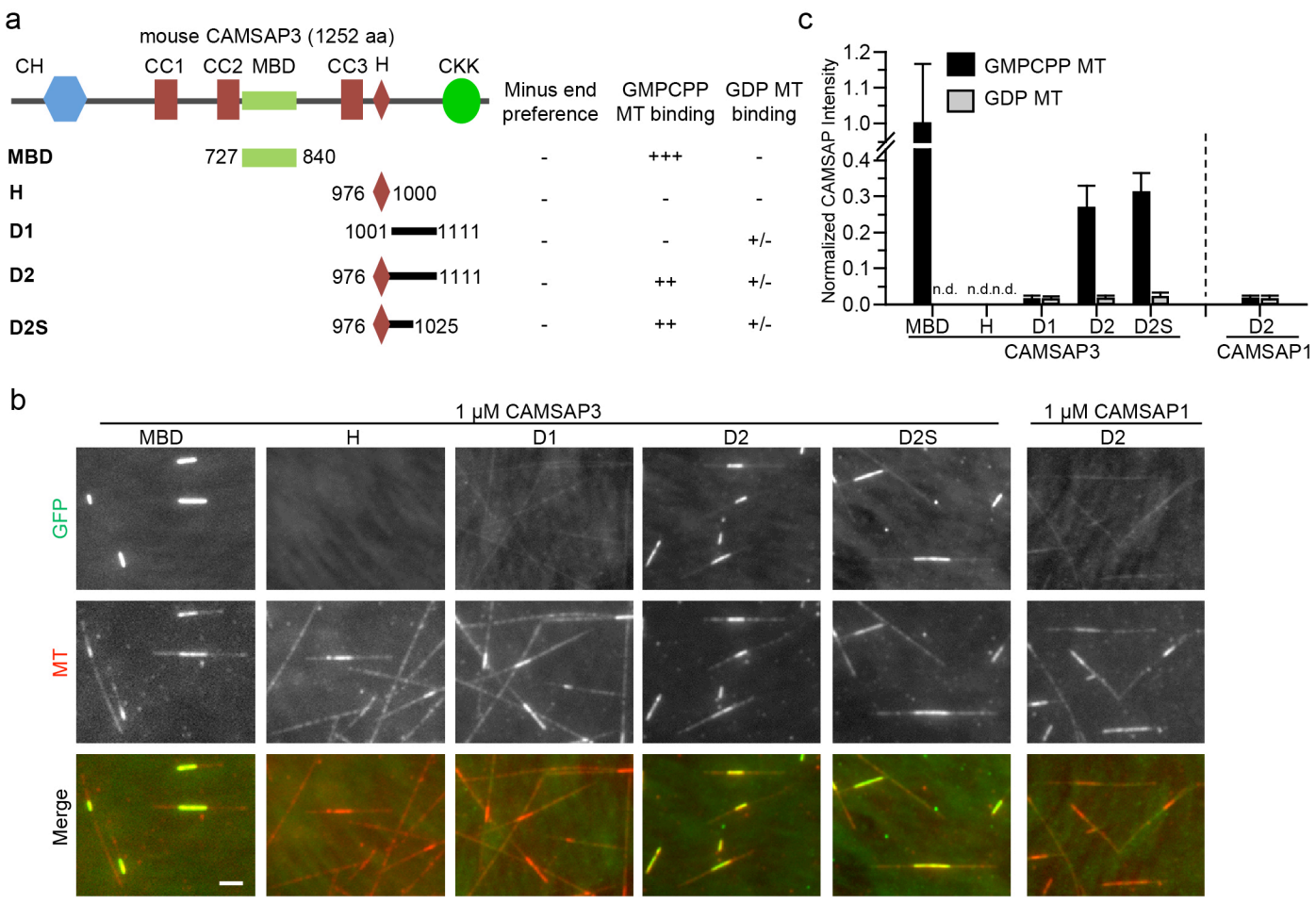

Supplementary Figure 1

C-terminal domains of CAMSAP3 do not confer MT minus end specificity.

(a) Schematic of the CAMSAP3 domain organization and the constructs used.

(b,c) TIRFM images and quantification of the binding of GFP-CAMSAP3 fragments to GMPCPP-stabilized MTs and dynamic GDP-MTs; values for GFP- CAMSAP1-D2 quantified in the same way are shown for comparison. The intensity is normalized to the average intensity of MBD on GMPCPP MTs. Scale bar, 2 µm.

(d) Sequence alignment of the linker region located upstream of the third coiled-coil in vertebrate CAMSAP1. Negatively and positively charged residues are highlighted in purple and cyan, respectively.

See also Supplementary Table 2.

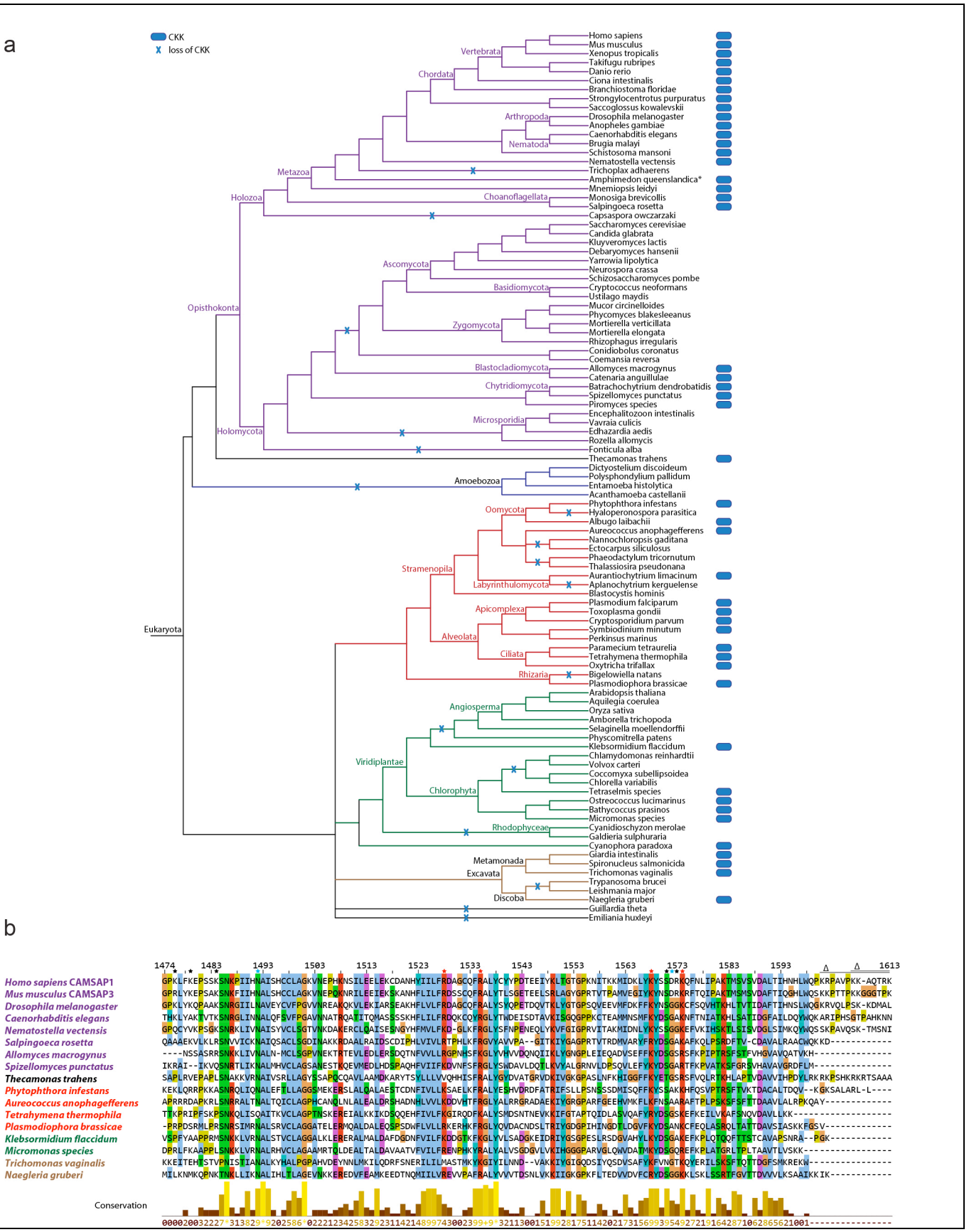
a
CKK
loss of CKK
Eukaryota
Opisthokonta
Amoebozoa
Holozoa
Holomycota
Metazoa
Chordata
Vertebrata
Arthropoda
Nematoda
Choanoflagellata
Ascomycota
Basidiomycota
Zygomycota
Blastocladiomycota
Chytridiomycota
Microsporidia
Homo sapiens
Mus musculus
Xenopus tropicalis
Takifugu rubripes
Danio rerio
Ciona intestinalis
Branchiostoma floridae
Strongylocentrotus purpuratus
Saccoglossus kowalevskii
Drosophila melanogaster
Anopheles gambiae
Caenorhabditis elegans
Brugia malayi
Schistosoma mansoni
Nematostella vectensis
Trichoplax adhaerens
Amphimedon queenslandica*
Mnemiopsis leidyi
Monosiga brevicollis
Salpingoeca rosetta
Capsaspora owczarzaki
Saccharomyces cerevisiae
Candida glabrata
Kluyveromyces lactis
Debaryomyces hansenii
Yarrowia lipolytica
Neurospora crassa
Schizosaccharomyces pombe
Cryptococcus neoformans
Ustilago maydis
Mucor circinelloides
Phycomyces blakesleeanus
Mortierella verticillata
Mortierella elongata
Rhizophagus irregularis
Conidiobolus coronatus
Coemansia reversa
Allomyces macrogynus
Catenaria anguillulae
Batrachochytrium dendrobatidis
Spizellomyces punctatus
Piromyces species
Encephalitozoon intestinalis
Vavraia culicis
Edhazardia aedis
Rozella allomycis
Fonticula alba
Thecamonas trahens
Dictyostelium discoideum
Polysphondylium pallidum
Entamoeba histolytica
Acanthamoeba castellanii
Stramenopila
Oomycota
Labyrinthulomycota
Phytophthora infestans
Hyaloperonospora parasitica
Albugo laibachii
Aureococcus anophagefferens
Nannochloropsis gaditana
Ectocarpus siliculosus
Phaeodactylum tricornutum
Thalassiosira pseudonana
Aurantiochytrium limacinum
Aplanochytrium kerguelense
Blastocystis hominis
Alveolata
Apicomplexa
Ciliata
Rhizaria
Plasmodium falciparum
Toxoplasma gondii
Cryptosporidium parvum
Symbiodinium minutum
Perkinsus marinus
Paramecium tetraurelia
Tetrahymena thermophila
Oxytricha trifallax
Bigelowiella natans
Plasmodiophora brassicae
Viridiplantae
Angiosperma
Chlorophyta
Rhodophyceae
Arabidopsis thaliana
Aquilegia coerulea
Oryza sativa
Amborella trichopoda
Selaginella moellendorffii
Physcomitrella patens
Klebsormidium flaccidum
Chlamydomonas reinhardtii
Volvox carteri
Coccomyxa subellipsoidea
Chlorella variabilis
Tetraselmis species
Ostreococcus lucimarinus
Bathycoccus prasinos
Micromonas species
Cyanidioschyzon merolae
Galdieria sulphuraria
Cyanophora paradoxa
Metamonada
Excavata
Discoba
Giardia intestinalis
Spironucleus salmonicida
Trichomonas vaginalis
Trypanosoma brucei
Leishmania major
Naegleria gruberi
Guillardia theta
Emiliania huxleyi
b
Homo sapiens CAMSAP1
Mus musculus CAMSAP3
Drosophila melanogaster
Caenorhabditis elegans
Nematostella vectensis
Salpingoeca rosetta
Allomyces macrogynus
Spizellomyces punctatus
Thecamonas trahens
Phytophthora infestans
Aureococcus anophagefferens
Tetrahymena thermophila
Plasmodiophora brassicae
Klebsormidium flaccidum
Micromonas species
Trichomonas vaginalis
Naegleria gruberi
Conservation

Supplementary Figure 2

The CKK is a highly conserved MT minus-end tracking domain.

(a) The presence of CKK in extant eukaryotic lineages and its evolutionary history since LECA. The CKK domain can be found in four out of five eukaryotic supergroups: Eukaryotic supergroups are indicated by coloured branches (Opisthokonta: purple, Amoebozoa: blue, Stramenopila-Alveolata-Rhizaria (SAR): red, Archaeplastida: green, Excavata: brown). Species tree depicting all species comprising our eukaryotic proteome database and the presences of the CKK domain as well as its inferred losses. The presence of CKK in LECA and indicated subsequent loss events were inferred according to Dollo parsimony, which allows for only a single invention. Asterisk: sequence derived from NCBI. Note that in the oomycetes, the loss of CKK domain seems relatively recent, because *Phytophthora infestans* and *Albugo laibachii* contain CKK, but downy mildew *Hyaloperonospora parasitica* lacks it.

(b) Multiple sequence alignment of the CKK domain in a subset of the species in (a). The supergroups to which the species encoding these sequences belong are indicated by the name colours as in (a). The numbering of amino acids is based on human CAMSAP1 sequence. The colored asterisks indicate the amino acids, which, when mutated to alanine, alter the CAMSAP1$_{mini}$ signal at MT minus ends compared to wild type protein; red asterisk, signal reduced to less than 25%; black asterisk, signal reduced to 25-75%; cyan asterisk, signal increased above 100%.

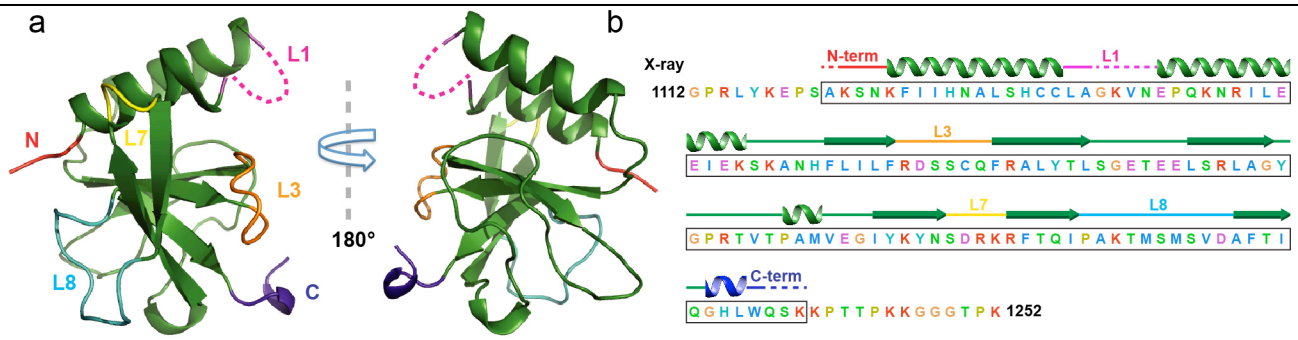

Supplementary Figure 3

The X-ray crystal structure of mouse CAMSAP3 CKK domain.

(a) Two views 180° apart of the ribbon representation of the *M. musculus* CAMSAP3 CKK domain crystal structure. Key loops as well as the N- and C-termini of the domain are labeled.

(b) The *M. musculus* CAMSAP3 CKK sequence, coloured according to side chain property, is shown, with overlying secondary structure based on our crystal structure. The boxed region indicates the construct used for X-ray crystallography. Secondary structure estimations deduced by X-ray crystallography are indicated above, colour coded consistent with the scheme in panel a, with unsolved regions indicated with dashed lines.

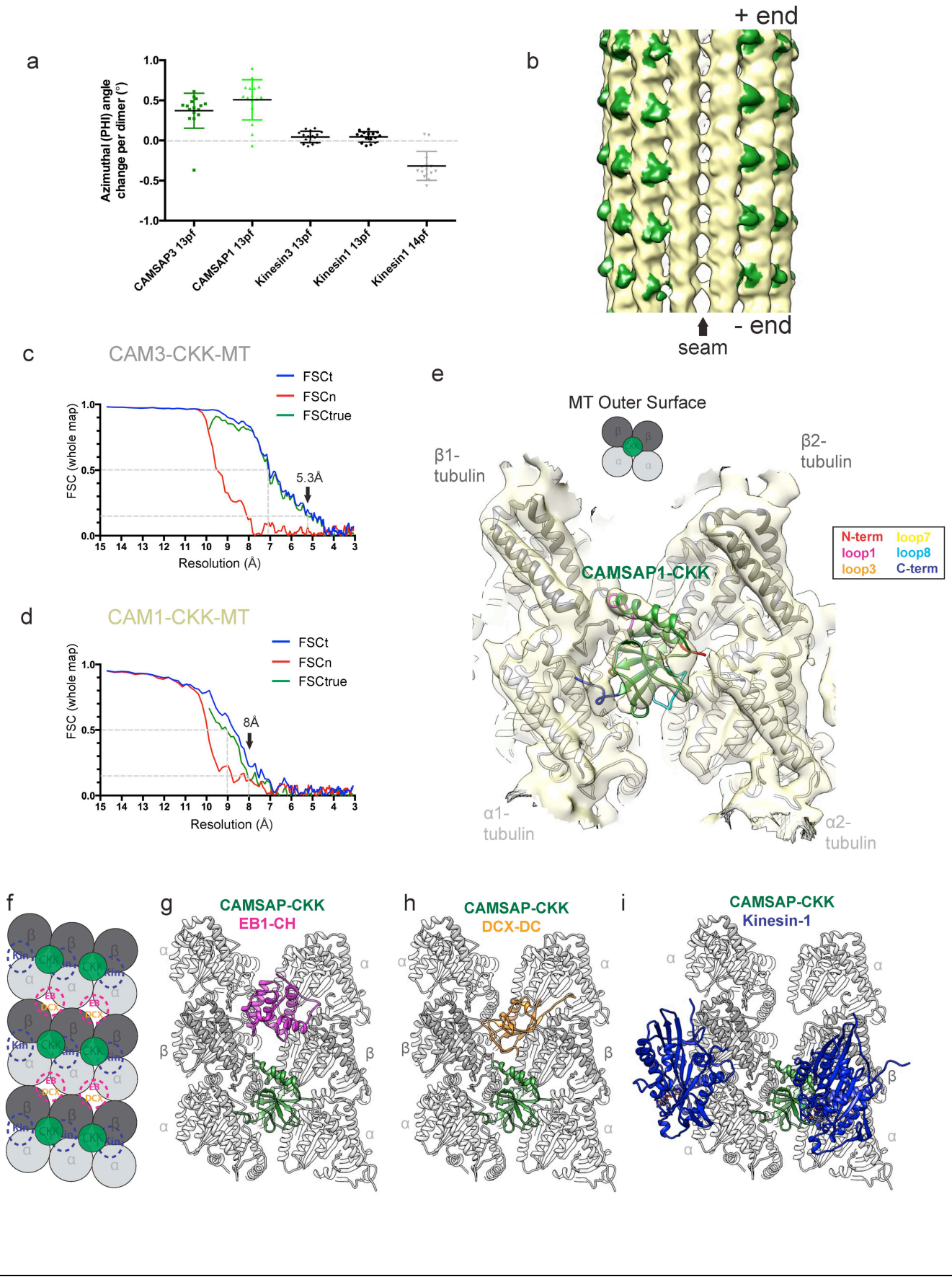
a
Azimuthal (PHI) angle change per dimer (°)
1.0
0.5
0.0
-0.5
-1.0
CAMSAP3 13pf
CAMSAP1 13pf
Kinesin3 13pf
Kinesin1 13pf
Kinesin1 14pf
b
+ end
- end
seam
c
CAM3-CKK-MT
FSCt
FSCn
FSCtrue
FSC (whole map)
5.3Å
Resolution (Å)
d
CAM1-CKK-MT
FSCt
FSCn
FSCtrue
FSC (whole map)
8Å
Resolution (Å)
e
MT Outer Surface
β1-tubulin
β2-tubulin
CAMSAP1-CKK
N-term
loop1
loop3
loop7
loop8
C-term
α1-tubulin
α2-tubulin
f
g
CAMSAP-CKK
EB1-CH
h
CAMSAP-CKK
DCX-DC
i
CAMSAP-CKK
Kinesin-1

Supplementary Figure 4

Evaluation of the resolution of CAMSAP-CKK MT reconstructions, conservation of the CKK binding site in CAMSAP1 and comparison of the CKK binding site with other MAPs and MT motors.

(a) Protofilament skew for 16 representative MTs from each dataset is depicted by plotting the average rotation angle around the MT axis (PHI) change per dimer moving axially towards the MT plus-end. CAMSAP CKK-decorated MTs are compared to control kinesin decorated paclitaxel-stabilized MTs (datasets from Atherton, J. *et al., eLife* **3**, e03680 ,2014). that show no skew for 13 pfs and a left-handed (negative) skew for 14pfs. PHI angles were determined in Frealign (Grigorieff, N., *Journal of structural biology* **157**, 117-125, 2007). CAMSAP CKK decorated 13pf MTs show right-handed (positive) skew, while control 13pf kinesin decorated MTs show little or no skew. In contrast, control 14pf kinesin decorated MTs show left-handed (negative) skew as expected (Chretien, D. & Wade, R.H., *Biology of the cell / under the auspices of the European Cell Biology Organization* **71**, 161-174, 1991). n=16 MTs per condition. Data represent mean ± SD. CAMSAP-3 13pf vs CAMSAP-1 13pf not significant, one-way ANOVA with Tukey's multiple comparison test. CAMSAP-3 13pf vs kinesin-3 13pf, $p<0.0001$. CAMSAP-3 13pf vs kinesin-1 13pf, $p<0.0001$. CAMSAP-1 13pf vs kinesin-3 13pf, $p<0.0001$. CAMSAP-1 13pf vs kinesin-1 13pf, $p<0.0001$.

(b) The asymmetric reconstruction of the CAMSAP1-CKK decorated 13pf taxol-stabilized MT low-pass filtered to 15Å resolution shows extra densities (green) every 8 nm corresponding to the CAMSAP1-CKK domain, which are absent at the seam (arrow).

(c, d) Fourier shell correlation (FSC) curves utilizing the gold-standard noise substitution method (Chen, S. *et al., Ultramicroscopy* **135**, 24-35, 2013) give an overall resolution estimate for the (c) CAMSAP3-CKK-MT reconstruction of 5.3Å and (d) CAMSAP1-CKK-MT reconstruction of 8Å.

(e) The averaged reconstruction of the CAMSAP1-CKK domain viewed from the MT surface contacting two β-tubulins and two α-tubulins at the intra-dimer, inter-protofilament interface. The CAMSAP-1 CKK is colored as in the CAMSAP3-CKK. α-tubulin is shown in light grey and β-tubulin is shown in dark grey. Above, schematic.

(f-i) Schematic depiction of the CKK binding site compared to other known MT binding partners, and structural models of (g) CAMSAP-CKK and EB1-CH domain (based on PDB ID 3JAK, *Zhang et al.,* E. *Cell* **162**, 849-859, 2015) (h) CAMSAP-CKK and DCX-DC domain (same binding site as EB, based on PDB ID 2XRP, Fourniol, F.J. *et al.*, *The Journal of cell biology* **191**, 463-470, 2010) and (i) CAMSAP-CKKs and kinesin-1 motor domain (based on PDB ID 4UY0, Atherton, J. *et al., eLife* **3**, e03680 ,2014, note steric overlap).

See also Supplementary Table 2.

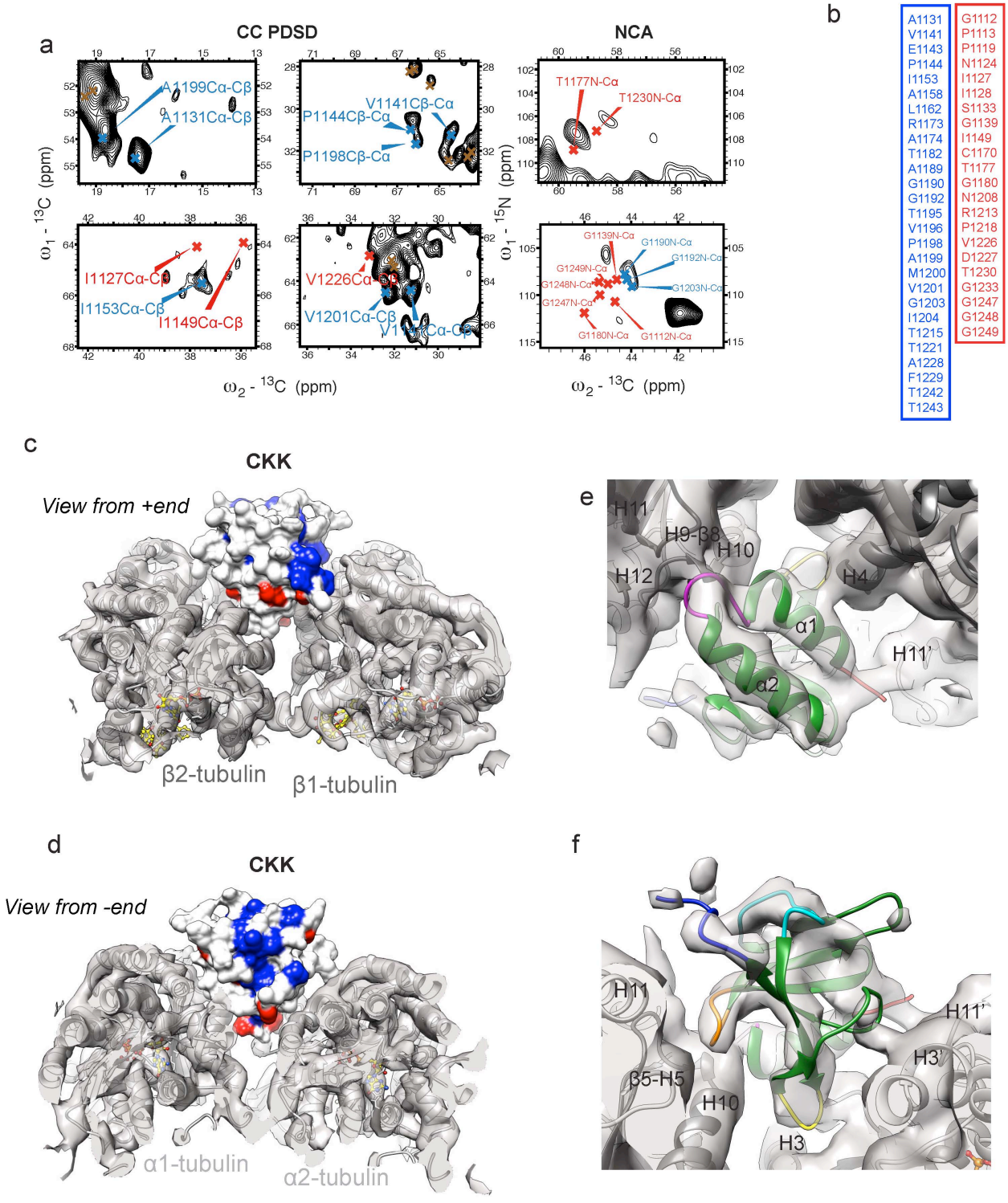

Supplementary Figure 5

Details of the CKK-MT binding site by ssNMR and cryo-EM.

(a) Zooms of well-resolved regions in the solid-state ^{13}C-^{13}C (PDSD, left and middle panels) and NCA (right panel) ssNMR spectra of [^{15}N,^{13}C,] labeled CKK bound to MTs. Crosses indicate expected signals based on solution-state chemical shifts of free CKK in solution. Signals for which a good match is found between expected and observed chemicals shifts are indicated in blue, while the absence of a corresponding signal is indicated in red. Brown crosses correspond to expected signals in overlapping regions.

(b) Full list of affected (red) and unaffected (blue) residues based on the NMR data.

(c, d) View from the MT plus-end (c) or minus-end (d) of the MT-bound CKK, reporting on ssNMR data obtained on [^{13}C,^{15}N] labeled CKK decorated MTs relative to NMR results on free CKK. The CKK is shown as a color-coded surface representation whilst a ribbon representation of the MT (light grey for α-tubulin and dark grey for β-tubulin) is shown within its respective grey transparent solid cryo-EM density. CKK residues that underwent significant chemical-shift/intensity changes are colored in red (affected) and those that experienced no change are indicated in blue (unaffected). White residues were not analysed due to signal overlap.

(e) A view from the plus end of the MT, showing details of the tubulin contacts of the CKK N-terminus (red), helix α1, loop1 (magenta) and loop7 (yellow), colored as in Fig. 2d. The experimental density is shown as transparent solid, with tubulin shown as grey ribbons fitted into the experimental density.

(f) A view from the minus end of the MT, showing details of the tubulin contacts of the CKK N-terminus (red), loop7 (yellow), the C-terminus (blue) loop3 (orange) and the position of loop8 (cyan).

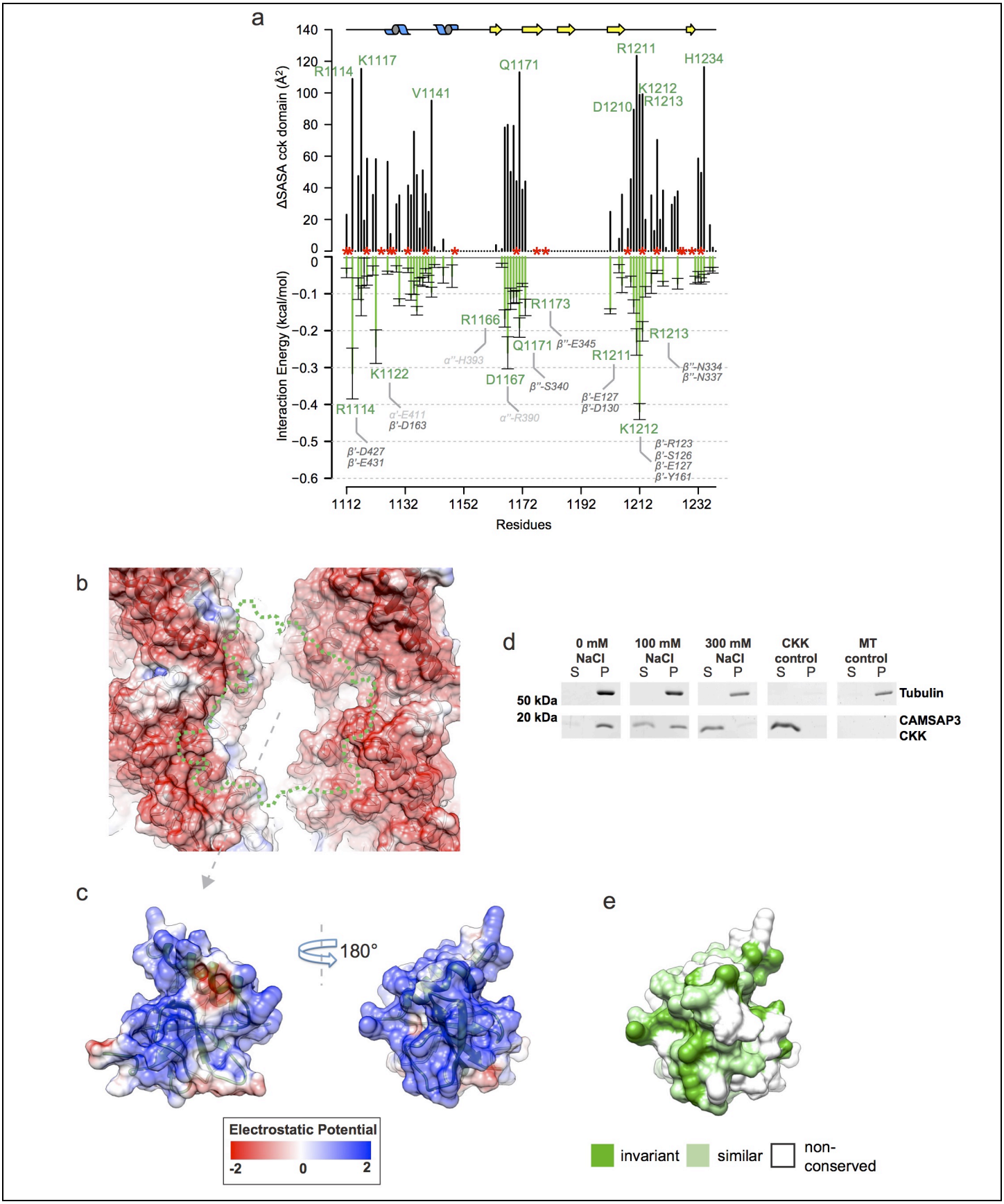
a
ΔSASA cck domain (Å²)
Interaction Energy (kcal/mol)
Residues
R1114
K1117
V1141
Q1171
R1211
H1234
K1212
R1213
D1210
R1166
R1173
Q1171
β''-E345
α''-H393
R1211
R1213
β''-N334
β''-N337
K1122
D1167
β''-S340
β'-E127
β'-D130
α''-R390
R1114
α'-E411
β'-D163
K1212
β'-D427
β'-E431
β'-R123
β'-S126
β'-E127
β'-Y161
b
c
180°
Electrostatic Potential
-2
0
2
d
0 mM NaCl
100 mM NaCl
300 mM NaCl
CKK control
MT control
S P
50 kDa
20 kDa
Tubulin
CAMSAP3 CKK
e
invariant
similar
non-conserved

Supplementary Figure 6

Characterization of the CKK-MT binding site; energetics and electrostatic contributions.

(a) CAMSAP3 residue-wise variation in solvent accessible surface area (top, black bars) and energetic contributions to MT binding (bottom, green bars). Selected CKK residues showing major solvent accessibility changes and energetic contributions are labelled in green, with corresponding interacting tubulin residues labelled in light grey for α-tubulin and dark grey for β-tubulin. Red stars indicate the location of residues with ssNMR signal shifts. Energetic contributions were determined from molecular dynamics simulations using the Amber MMGBSA routine. Data represent mean ± SD. Solvent accessibility was determined with Bio3D (Grant, B.J. et al., *Bioinformatics* **22**, 2695-2696, 2006, see Methods).

(b) Surface representation of the MT-CKK interface on tubulin colored by electrostatic potential, with the CKK binding site indicated by a green dashed outline. The surface was calculated with the APBS (Baker, N.A. *et al., PNAS* **98**, 10037-10041, 2001) and pdb2pqr (Dolinsky, T.J. *et al., Nucleic acids research* **35**, W522-525, 2007).

(c) The corresponding front view of the surface-represented CKK (left) colored in the same way as panel b, while a 180° rotation of this view illustrating the tubulin-facing surface of the CKK is shown on the right.

(d) MT pelleting assay, in which the CAMSAP3 CKK and MTs were mixed in equimolar ratios at different salt concentrations in BRB35 buffer. As controls, the CKK domain and MTs were processed alone. The supernatants (S) and pellets (P) were separated on a 15 % SDS-PAGE and stained with Coomassie.

(e) Tubulin-facing surface representation of CAMSAP3 CKK surface showing the residue conservation between the *M. musculus*, *C. elegans*, *D. melanogaster* CKK domains. Dark green, invariant residues; light green, similar residues; white, non-conserved residues. Equivalent view to right hand image in panel (c) is shown.

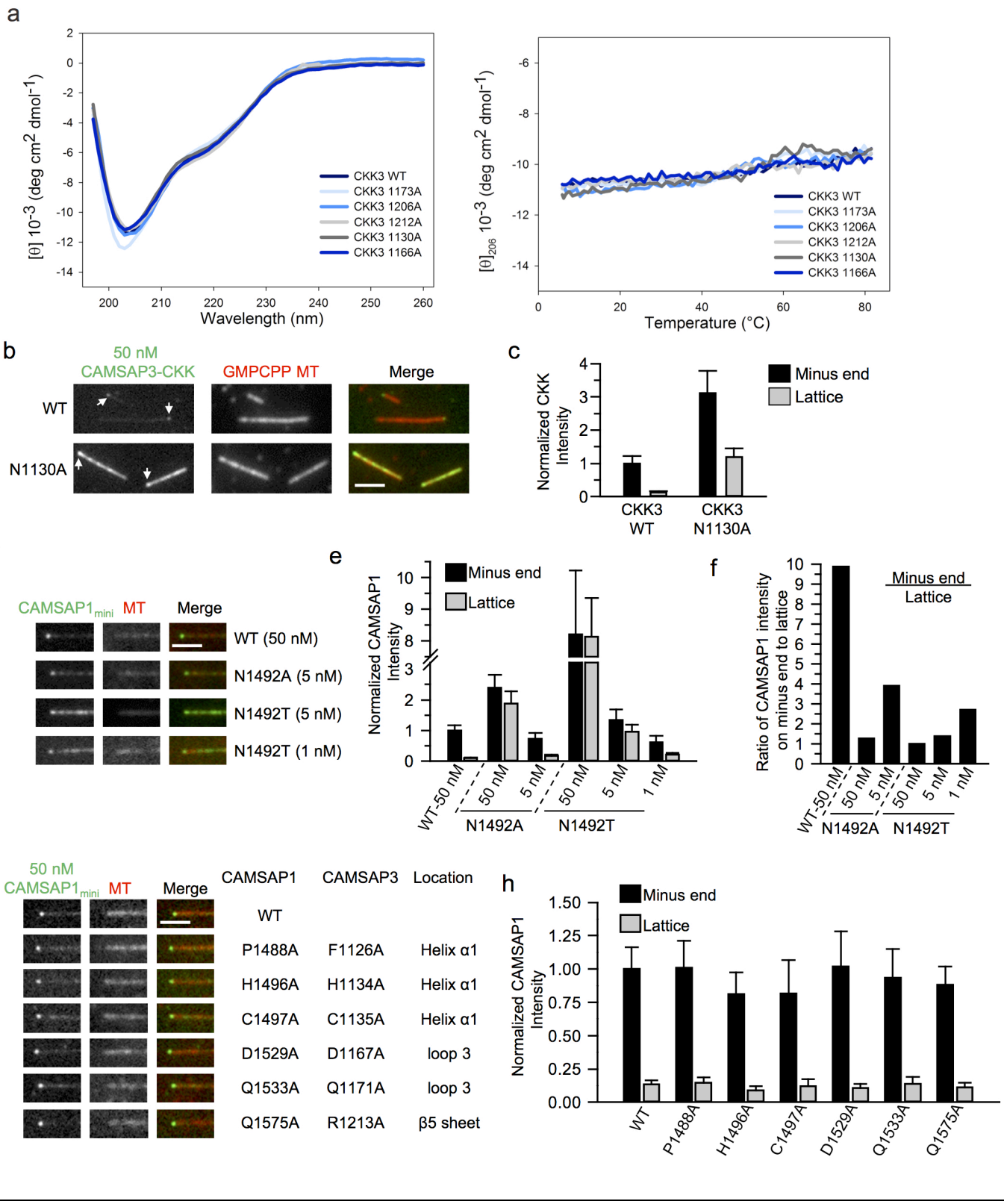
a
[θ] 10-3 (deg cm2 dmol-1)
Wavelength (nm)
CKK3 WT
CKK3 1173A
CKK3 1206A
CKK3 1212A
CKK3 1130A
CKK3 1166A
[θ]206 10-3 (deg cm2 dmol-1)
Temperature (°C)
b
50 nM CAMSAP3-CKK
GMPCPP MT
Merge
WT
N1130A
c
Normalized CKK Intensity
Minus end
Lattice
CKK3 WT
CKK3 N1130A
d
CAMSAP1mini
MT
Merge
WT (50 nM)
N1492A (5 nM)
N1492T (5 nM)
N1492T (1 nM)
e
Normalized CAMSAP1 Intensity
Minus end
Lattice
WT-50 nM
50 nM
5 nM
50 nM
5 nM
1 nM
N1492A
N1492T
f
Ratio of CAMSAP1 intensity on minus end to lattice
Minus end
Lattice
WT-50 nM
50 nM
5 nM
50 nM
5 nM
1 nM
N1492A
N1492T
g
50 nM CAMSAP1mini
MT
Merge
CAMSAP1 CAMSAP3 Location
WT
P1488A F1126A Helix α1
H1496A H1134A Helix α1
C1497A C1135A Helix α1
D1529A D1167A loop 3
Q1533A Q1171A loop 3
Q1575A R1213A β5 sheet
h
Normalized CAMSAP1 Intensity
Minus end
Lattice
WT
P1488A
H1496A
C1497A
D1529A
Q1533A
Q1575A

Supplementary Figure 7

Validation of CKK-MT contact sites using CKK mutants.

(a) CD spectra (left) and thermal unfolding profiles (right) of CAMSAP3 CKK variants. The spectra were recorded at 5 °C in PBS at a protein concentration of 0.25 mg/ml. The thermal unfolding profiles were recorded at 206 nm.

(b,c) TIRFM images and quantification of GFP-CAMSAP3 CKK and N1130A mutant binding to GMPCPP-stabilized MTs. The intensity is normalized to the average minus-end intensity of WT. Similar to CAMSAP1 N1492A mutant, CAMSAP3 N1130A mutant shows increased MT lattice binding. n=80 MTs.

(d-f) TIRFM images and quantifications of the binding of GFP-CAMSAP1$_{mini}$ N1492A and N1492T mutants to the minus ends and lattice of dynamic MTs at different concentrations. Both mutants show minus-end specificity at lower concentrations (see Fig. 4a,d for images at 50 nM). The intensity is normalized to the average minus-end intensity of wild type. n=30-50 MTs. The data for N1492A and N1492T mutants at 50 nM was replotted from Fig. 4d.

(g,h) TIRFM images and quantification of binding of GFP-CAMSAP1$_{mini}$ and mutants to the minus ends and lattice of dynamic MTs. The intensity is normalized to the average minus-end intensity of wild type. n=30 MTs.

Scale bars, 1 μm. Data represent mean ± SD.

See also Supplementary Table 2.

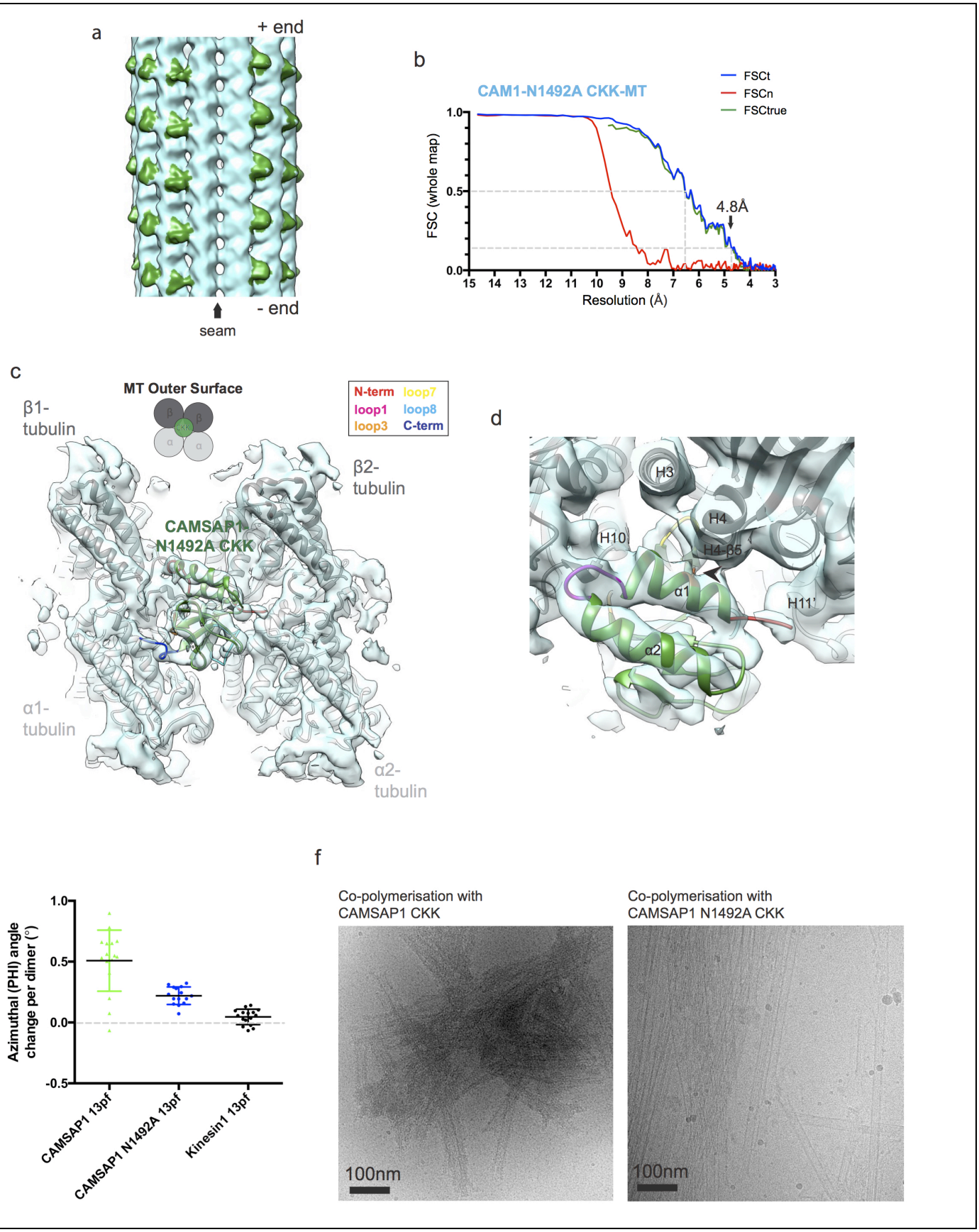
a
+ end
- end
seam
b
CAM1-N1492A CKK-MT
FSCt
FSCn
FSCtrue
FSC (whole map)
1.0
0.5
0.0
4.8Å
15 14 13 12 11 10 9 8 7 6 5 4 3
Resolution (Å)
c
MT Outer Surface
β1-
tubulin
β2-
tubulin
CAMSAP1-
N1492A CKK
α1-
tubulin
α2-
tubulin
N-term
loop1
loop3
loop7
loop8
C-term
d
H3
H4
H10
H4-β5
α1
H11'
α2
e
Azimuthal (PHI) angle
change per dimer (°)
1.0
0.5
0.0
-0.5
CAMSAP1 13pf
CAMSAP1 N1492A 13pf
Kinesin1 13pf
f
Co-polymerisation with
CAMSAP1 CKK
Co-polymerisation with
CAMSAP1 N1492A CKK
100nm
100nm

Supplementary Figure 8

Reconstruction of the CAMSAP1-N1492A CKK mutant and analysis of the effect of CKK on MT polymerization.

(a) The asymmetric reconstruction of the CAMSAP1-N1492A CKK decorated 13pf paciltaxel-stabilized MT low-pass filtered to 15Å resolution shows extra densities (green) every 8nm corresponding to the CAMSAP1-N1492A CKK domain, which are absent at the seam similar to wild type (arrow).

(b) FSC curves utilizing the gold-standard noise substitution method (Chen, S. *et al., Ultramicroscopy* **135**, 24-35, 2013) give an overall resolution estimate for the CAMSAP1-N1492A CKK-MT reconstruction of 4.8Å.

(c) The averaged reconstruction of the CAMSAP1- N1492A CKK domain viewed from the MT surface contacting two β-tubulins and two α-tubulins at the intra-dimer, inter-protofilament interface. The CAMSAP1-N1492A CKK is colored as previously. α-tubulin is shown in light grey and β-tubulin is shown in dark grey. Cryo-EM density is shown as transparent light blue solid. Above, schematic.

(d) View from the plus end of the CAMSAP1-N1492A CKK decorated 13pf MT, showing details of the tubulin contacts of the N-terminus (red), helix α1, loop1 (magenta) and loop 7 (yellow), colored as in Supplementary Fig. 5e. The position of N1492A (brown) is also indicated (arrowhead). The experimental density is shown as blue transparent solid, with tubulin shown as grey ribbons fitted into the experimental density.

(e) Protofilament skew for representative MTs from each dataset is depicted as in Supplementary Figure 4a. The reduced skew produced by CAMSAP1-N1492A CKK-decorated MTs are compared to wild type CKK MTs and control kinesin decorated paclitaxel-stabilized MTs (datasets from Atherton, J. *et al., eLife* **3**, e03680 ,2014). For CAMSAP1 CKK, n=16, for kinesin1 decorated MTs, n=16; for CAMSAP1-N1492A CKK-decorated MTs, n=15. Data represent mean ± SD. 1-way ANOVA, CAMSAP1 CKK N1492A vs CAMSAP1 CKK wild type, $p<0.001$;CAMSAP1 CKK N1492A vs kinesin-1 13pf $p<0.05$.

(f) Copolymerisation of tubulin with CAMSAP1 CKK domain yields few MTs but produces clumps of heterogeneous tubulin oligomers (left), while copolymerisation with CAMSAP-N1492A yields mainly MTs (right). Representative cryo-EM images of the products of each polymerisation reaction are shown.

See also Supplementary Table 2.

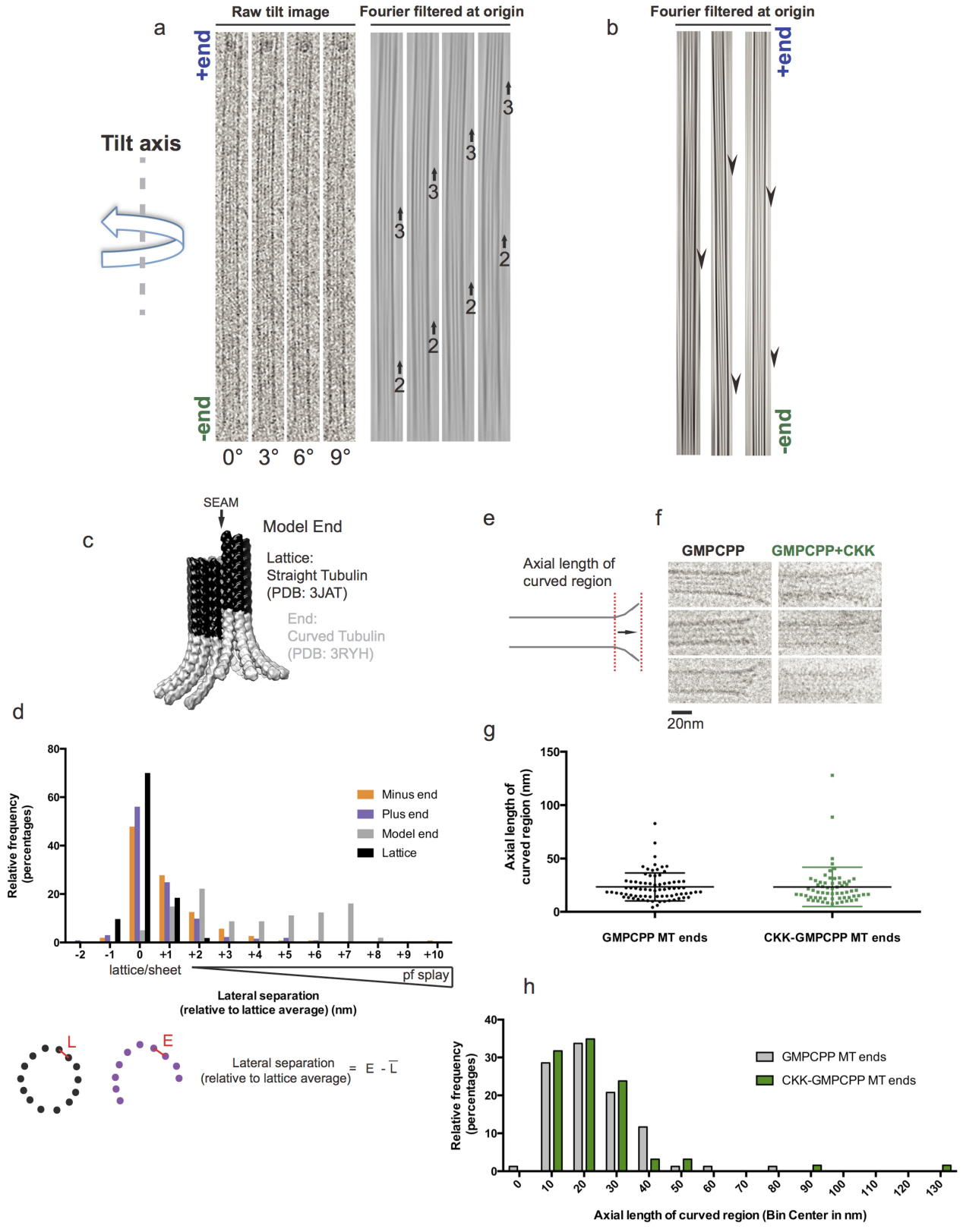
a
Raw tilt image
Fourier filtered at origin
+end
-end
Tilt axis
0° 3° 6° 9°
b
Fourier filtered at origin
+end
-end
c
SEAM
Model End
Lattice:
Straight Tubulin
(PDB: 3JAT)
End:
Curved Tubulin
(PDB: 3RYH)
d
Relative frequency (percentages)
Minus end
Plus end
Model end
Lattice
lattice/sheet
pf splay
Lateral separation
(relative to lattice average) (nm)
L
E
Lateral separation
(relative to lattice average) = E - L
e
Axial length of
curved region
f
GMPCPP
GMPCPP+CKK
20nm
g
Axial length of curved region (nm)
GMPCPP MT ends
CKK-GMPCPP MT ends
h
Relative frequency (percentages)
GMPCPP MT ends
CKK-GMPCPP MT ends
Axial length of curved region (Bin Center in nm)

Supplementary Figure 9

Determination of MT polarity in cryo-tomograms.

(a) The moire pattern from successive raw images in a representative tilt series, and corresponding Fourier filtered images. The tilt method (Chretien, D. *et al., Structure* **4**, 1031-1040, 1996) uses the position of the tilt axis and shift with tilt of the fringes (2 and 3) in the moiré pattern of 14pf MTs to identify MT polarity. The plus (+) end is oriented towards the top of the page.

(b) The moiré pattern of a subset of Fourier filtered MT projections also contain an arrowhead pattern, which arises from pf skew, which can be used to corroborate MT polarity (Chretien, D. *et al., Structure* **4**, 1031-1040, 1996). In 14pf MTs, the arrowheads point towards the minus end; black arrowheads indicate the position of the arrowhead moire patterns on the MTs and thus demonstrate that the MTs are oriented with their plus ends towards the top of the image.

(c) 14 pf MT minus end model built from known tubulin dimer structures (PDB numbers indicated).

(d) Change in lateral pf separation compared to lattice was measured in transverse sections of the MT lattice and ends and plotted as frequency histogram (% of total observations). At both minus and plus ends, most pfs remain laterally closely associated despite longitudinal curvature (0 or +1 nm separation), consistent with a sheet-like structure, and in contrast to the lateral separation of the end model where pfs instead splay apart. Inset; a schematic of a transverse section through the MT lattice and an MT end indicating pf lateral separation distance in the lattice (L) and in the longitudinally curved end region (E).

(e) A scheme illustrating the curved region of a MT end in 2D. The measured axial length of the curved region is the distance between the two red dashed lines.

(f) Gallery of 2D projections of exemplar GMPCPP MT ends with or without 1.5 mg/ml CAMSAP3 CKK domain. Note similar end structures with moderate longitudinal curvature, but also the much higher background in the presence of excess CKK protein.

(g) 2D quantification of the axial length of curved regions of GMPCPP MT ends (as shown in panel e) in the presence or absence of CAMSAP3 CKK domain. No significant difference is observed with added CKK domain, two-tailed Mann-Whitney U test. For GMPCPP-MT ends, n=77 MT ends; for CKK-GMPCPP-MT ends, n=63 MT ends. Data represent mean ± SD.

(h) A histogram of axial length of curved regions of GMPCPP MT ends shows similar length distributions in the presence or absence of CAMSAP3 CKK domain. In both cases, the most common bin center of end lengths is 20 nm (bin width 10 nm).

See also Supplementary Table 2.